Civil Engineering and Applied Solutions

Research Article

journal homepage: ceas.journals.umz.ac.ir

CEAS Civil Engineering and Applied Solutions

Experimental Study of Circular Concrete Column Confined with Hybrid FRP-Steel Tube Under Axial Load

Abolghasem Salari [a], Morteza Naghipour [a*]

[a] *Faculty of Civil Engineering, Babol Noshirvani University of Technology, Babol, Iran*

ARTICLE INFO

Keywords:
Concrete column
Confinement
Stress-strain curve
Steel
FRP
Steel-FRP composite tube

Article history:
Received 8 May 2025
Accepted 13 May 2025
Available online 01 July 2025

ABSTRACT

This study investigates the axial compressive behavior of circular concrete columns confined using three methods: steel tube confinement, FRP confinement, and hybrid FRP–steel tube confinement. Specimens were designed with similar confinement ratios to allow fair evaluation of their mechanical performance. Experimental results showed that while the type of confinement had little effect on initial stiffness, it significantly influenced the post-peak behavior. Steel confinement offered the highest strength and ductility, while FRP confinement increased ultimate strain but failed abruptly due to brittle rupture. The hybrid system exhibited a staged failure mechanism with improved confinement efficiency and a balance between strength and ductility. Stress–strain curves, volumetric strain trends, and tangent Poisson's ratio analyses highlighted the superior performance of hybrid systems. The findings suggest that hybrid FRP–steel confinement is a promising solution for enhancing both strength and deformation capacity in reinforced concrete columns, especially in seismic or high-performance structural applications.

1. Introduction

Concrete is one of the most widely used materials in structural engineering due to its high compressive strength, availability, and cost-effectiveness. However, its brittle nature and low tensile capacity make it vulnerable to axial loads, especially in seismic zones or heavily loaded structures. To overcome these limitations, various confinement techniques have been developed to enhance the mechanical performance of concrete elements, particularly columns. When an axial compressive force is applied to a concrete column, lateral expansion occurs due to the Poisson effect. Introducing a confining material restricts this expansion and induces lateral pressure on the core, transforming the stress state of the concrete from uniaxial to triaxial. As a result, confined concrete exhibits improved energy absorption and deformation capacity.

One of the earliest and most influential models in this field was proposed by Richartet al. [1] through experimental investigations on concrete cylinders under combined compressive stresses. Their study demonstrated that applying lateral confining pressure significantly increases the axial compressive strength of concrete. Building on this, Newman and Newman [2] proposed a more realistic basis for design, especially in situations involving moderate to high levels of active confinement. A significant advancement came with the work of Mander et al. [3], who proposed a widely used stress–strain model for steel-confined concrete that effectively captures strength and ductility improvements, especially in seismic applications. Han et al. [4] highlighted the significant influence of geometry and loading conditions on the confinement efficiency of steel tube-confined stub columns under localized axial loads. Liu et al. [5] confirmed that steel tubes provide effective lateral confinement, significantly enhancing the strength and ductility of CTRC columns. Qi et al. [6] emphasized the influence of geometry, showing that thicker tube walls and shorter column heights improve confinement by reducing buckling and increasing lateral restraint. Lin et al. [7] found that in circular concrete-filled steel tube columns, confinement effectiveness and compressive strength depend on the stress path at low confinement levels, but become path-independent as confinement increases. Xiamuxi et al. [8] investigated the effect of steel tube wall thickness on the axial

* Corresponding author.
E-mail addresses: m-naghi@nit.ac.ir (M. Naghipour).

https://doi.org/10.22080/ceas.2025.29200.1011
ISSN: 3092-7749/
How to cite this article: Salari ,A., Naghipour, M. Experimental study of circular concrete column confined with hybrid FRP-steel tube under axial load. Civil Engineering and Applied Solutions. 2025; 1(2): 1–13. doi:10.22080/ceas.2025.29200.1011.

compression behavior of square columns filled with reinforced and recycled aggregate concrete. They found that increasing wall thickness enhances confinement, improves load-bearing capacity, and delays failure, underscoring the importance of steel tube confinement in structural performance. Cao et al. [9] showed that steel tube confinement enhances concrete durability by reducing sulfate penetration and cracking.

While steel confinement offers reliable confinement capacity, FRP has emerged as a promising alternative. Kurt [10] found that PVC tubes offered minimal confinement due to low stiffness, while Harmon [11] showed that FRP tubes (CFRP and GFRP) provided effective confinement, with bilinear stress–strain behavior influenced by fiber volume ratio. Lam et al. [12] studied the axial behavior of FRP-confined concrete under cyclic and monotonic compression. Their results showed that cyclic loading had minimal effect on the stress–strain curve envelope but caused a slight increase in ultimate axial strain. Berthet et al. [13] developed a model for FRP-confined concrete, showing that confinement efficiency depends on hoop behavior, concrete strength, and stiffness. Li et al. [14] found that fiber orientation significantly affects confinement efficiency. Hoop-aligned fibers (90°) provided the best strength and ductility, while axial (0°) and angled (45°) orientations led to earlier or mixed-mode failures, highlighting the importance of hoop-direction reinforcement. Toutanji et al. [15] showed that the axial strength of FRP-confined concrete columns increases with FRP jacket thickness and tensile strength. Elsanadedy et al. [16] investigated size effects in FRP-confined concrete and found that larger column diameters reduced compressive strength in unconfined concrete, though the effect was less pronounced in confined specimens. Yang et al. [17] developed an ultrasonic method to monitor damage in FRP-confined concrete, effectively detecting stiffness loss and rupture zones. Zheng et al. [18] identified the Wei and Wu model as the most accurate for predicting ultimate axial strain in FRP-confined non-circular columns.

While FRP confinement can significantly enhance axial capacity, its brittle failure mode often leads to sudden loss of confinement and abrupt column collapse. In contrast, steel tube confinement provides more gradual failure due to its elastic–plastic behavior and sustained lateral pressure after yielding. However, steel systems are vulnerable to issues such as corrosion and increased weight, limiting their long-term durability. Xiao et al. [19] demonstrated that combining steel tubes with external FRP layers improves strength, ductility, and seismic performance in concrete-filled steel tubular (CFT) column systems, though a gap between layers can delay FRP activation—underscoring the need for careful interface detailing. Feng et al. [20] showed that combining steel tubes with FRP-confined cores improves confinement, ductility, and residual strength in composite columns. Ma et al. [21] used the XGBoost algorithm to accurately predict the axial strength of CFRP-confined CFT columns. Their model outperformed other machine learning methods, achieving high accuracy ($R^2 = 0.9850$) after optimization. Liu et al. [22] proposed a machine learning-based framework using synthetic data to predict and optimize the axial strength of FRP-reinforced CFT columns. The model, combined with genetic algorithm optimization, outperformed traditional design methods and supports the efficient design of FRP-confined CFT systems.

To overcome the limitations of single-material confinement systems, this study investigates a hybrid FRP–steel tube confinement approach combining an inner steel tube with an outer FRP wrap. The experimental program included four groups of cylindrical specimens: unconfined concrete, steel tube-confined, FRP-confined, and hybrid FRP–steel tube-confined. All specimens were cast from a single concrete batch and designed with comparable confinement ratios to enable fair comparisons. Axial compression tests were conducted using a 200-ton capacity machine, with strain gauges and LVDTs installed to measure lateral and axial deformation. The hybrid system was designed to exploit the ductility of steel and the strength and corrosion resistance of FRP. This configuration aims to enhance compressive strength, ductility, and post-peak behavior while delaying brittle failure. The results are compared to assess the hybrid system's efficiency relative to steel- and FRP-only confinement

2. Experimental phase

2.1. Specimens

Four types of specimens were prepared: 1. Unconfined concrete cylinders (Group R-control samples), 2. Steel tube-confined cylinders (Group S), 3. FRP-confined cylinders (Group F), and 4-Hybrid steel + FRP-confined cylinders (Group SF). Each group consisted of multiple identical specimens; all cast from a single concrete batch to ensure uniformity. Fig. 1 shows the geometric properties of specimens. Each cylinder had a core diameter of 55 mm and a height of 140–150 mm, producing height-to-diameter ratios from 2.3 to 2.7. This ensured minimal buckling and friction effects (Table 1).

2.2. Confinement thickness

The configurations were selected to ensure that the confinement Ratio C_r values across groups are similar, enabling fair comparisons of their effectiveness. The confinement ratio is a dimensionless parameter that quantifies the level of lateral confinement pressure applied to the concrete core, normalized by the concrete's unconfined strength. It is defined as:

$$C_r = \frac{f_l}{f_c'} \tag{1}$$

where f_l is lateral confining pressure (from steel, FRP, or hybrid system), and f_c' is the unconfined compressive strength of concrete. The lateral confining pressure f_l depends on the thickness and stiffness of the confining material. This pressure can be estimated using hoop equilibrium theory. The lateral confining pressure f_l for steel tubes, FRP jackets, and hybrid confinement (steel + FRP) are defined in Eqs. 7 to 9, respectively:

$$f_l = \frac{2t_s f_{ys}}{D} \quad (2)$$

$$f_l = \frac{2t_f f_{uf}}{D} \quad (3)$$

$$f_l = \frac{2t_s f_{ys} + 2t_f f_{uf}}{D} \quad (4)$$

where t_s and f_{ys} are the thickness and yield strength of the steel tube, t_f and f_{uf} are the thickness and ultimate tensile strength of the FRP, and D is the internal diameter of the concrete core. The steel tube thickness was 2.0 mm for specimens in Group S, while Group F specimens were wrapped with two layers of FRP, totaling 0.32 mm in thickness. For the hybrid Group SF, specimens were confined using a 0.9 mm thick steel tube combined with a 0.16 mm thick single-layer FRP wrap (Fig. 2).

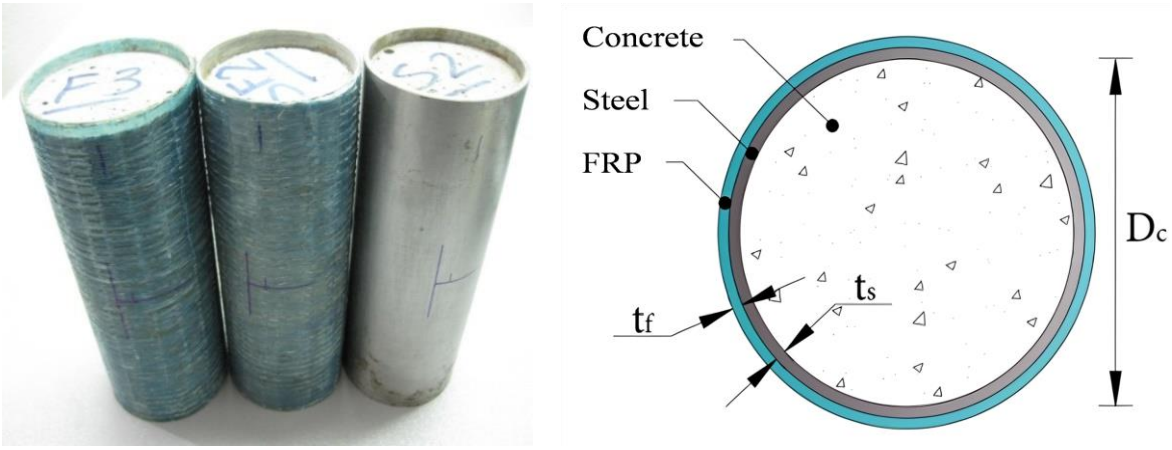

(a) (b)

Fig. 1. (a) Confined specimens, top view of a concrete column confined with a hybrid FRP–steel tube.

Table 1. Geometric Properties of Specimens.

Group	Core Diameter (mm)	Height (mm)	H/D Ratio	No. of Specimens
R (Control Samples)	55	150	2.7	6
S (Confined Specimens)	55	140	2.5	5
F (Confined Specimens)	60	140	2.3	5
SF (Confined Specimens)	55	140	2.5	5

Fig. 2. Hybrid steel–FRP tube before concrete casting.

2.3. Specimen preparation and curing conditions

Two days after casting, the control samples (Group R), which were not confined (Fig. 3(a)), were de-molded and placed in a water curing tank. These specimens remained fully submerged in water until the day of testing. Confined specimens, encased in steel tubes (Group S), FRP jackets (Group F), and hybrid steel–FRP tubes (Group SF), were not immersed in water after demolding. Because the lateral surfaces were covered with impermeable jackets and the top and bottom surfaces were sealed using steel end

plates, the risk of moisture loss was minimized (Fig. 3(b)). These specimens were stored at room temperature under sealed conditions until the day of testing.

Fig. 3. (a) Control specimens (Group R), (b) Confined specimens with steel tubes (Group S), FRP jackets (Group F), and hybrid steel–FRP tubes (Group SF).

To compare the unconfined compressive strength of the same concrete used in the confined specimens, on the test day, two specimens from each confined group were carefully cut and stripped of their steel or FRP jackets using a precision saw. The concrete core was then extracted and tested as a reference. These samples were labeled as unconfined specimens from jacketed groups (sometimes referred to as "stripped controls") and were used to directly measure the baseline strength of the confined groups' concrete without external confinement (Fig. 4).

Fig. 4. Concrete cores extracted from confined specimens.

2.4. Material properties

The materials used in this study included concrete, steel tubes, and fiber-reinforced polymer (FRP) jackets. The concrete was designed according to ACI 211 standards with a target compressive strength of 35 MPa. The steel used for confinement was tested and found to have a modulus of elasticity of 210 GPa and yield strength of 340 MPa. It also exhibited strain hardening, with an ultimate tensile strength of approximately 480 MPa. For external confinement, GFRP (Glass Fiber Reinforced Polymer) sheets were used. According to the manufacturer, the GFRP had a modulus of elasticity of 76 GPa and an ultimate tensile strength of 2300 MPa. The FRP jackets were manufactured using the wet lay-up process, and fibers were oriented in the hoop direction to provide effective lateral confinement.

2.5. Test setup and instrumentational

All specimens were tested using a 200-ton capacity ELE compression testing machine. For the control (unconfined) specimens, two MDF plates were placed at the top and bottom ends of the cylinders to reduce stress concentration and prevent premature cracking. The average compressive strength of the unconfined specimens was recorded and used as the reference strength f_c'. For the confined specimens (not acting as structural columns), the axial load was applied directly to the concrete core rather than through the confining shell. To ensure this, a steel rod with a diameter smaller than the inner diameter of the confining tube was used to apply load directly to the core. This ensured that no contact occurred between the loading platen and the inner surface of the confinement tube, preventing friction effects that could influence test results. The loading and instrumentation setup is shown in

Fig. 5.

Fig. 5. A steel-confined specimen with instrumentation for loading and deformation measurement.

To measure lateral strain, two horizontal strain gauges were symmetrically mounted on opposite sides of each specimen at mid-height on the external surface (as shown in Fig. 6(a)). The average reading from these gauges was taken as the lateral strain. Additionally, to evaluate the stress distribution and possible circumferential cracking in the tube, a vertical strain gauge was added to one of the horizontal gauges. To determine the axial strain of the concrete core, two LVDTs were placed symmetrically on opposite sides of each specimen. The average displacement recorded by these LVDTs was taken as the vertical deformation (see Fig. 6(b) for the test setup).

(a)

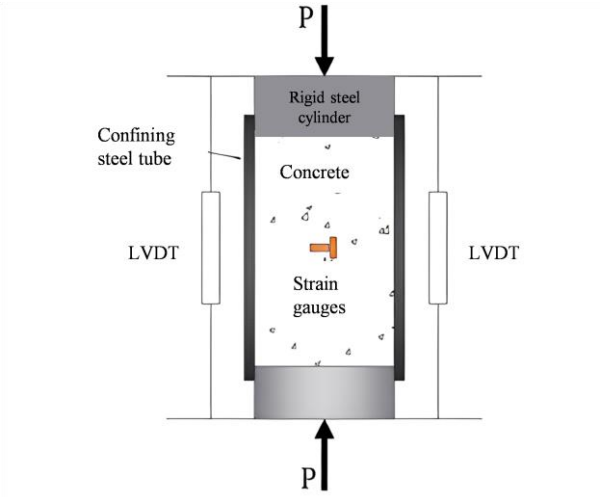

(b)

Fig. 6. (a) Strain gauge arrangement on confined specimens, (b) Loading setup for confined specimens.

3. Results and discussion

3.1. Failure mode

3.1.1.Unconfined concrete specimens (Group R)

Fig. 7 shows the failure pattern of control specimens cured in water. The observed failures correspond primarily to Type B and Type C modes in ASTMC39. These refer to conical shear failure and shear with splitting, respectively. The cracks observed in the specimens were relatively deep, and in some cases, the failure was accompanied by a distinctly loud sound, indicating brittle fracture through the aggregate particles. This confirms that the failure was not limited to the cement paste but involved the fracture of coarse aggregates, typical of well-cured, high-strength concrete.

Fig. 7. Failure patterns of reference concrete specimens.

Further, two specimens from each confined group were tested after removing their steel or FRP confinement on the day of testing. As shown in Fig. 8, the resulting failure was characterized by very fine surface cracks with no significant crack depth or audible fracture sound, indicating low-energy brittle failure. The cracks did not propagate through the coarse aggregates, suggesting that the failure occurred primarily along the weakened cement paste–aggregate interface. This brittle response confirms the limited integrity of the exposed concrete cores, likely due to micro-damage during confinement removal and the absence of external restraint.

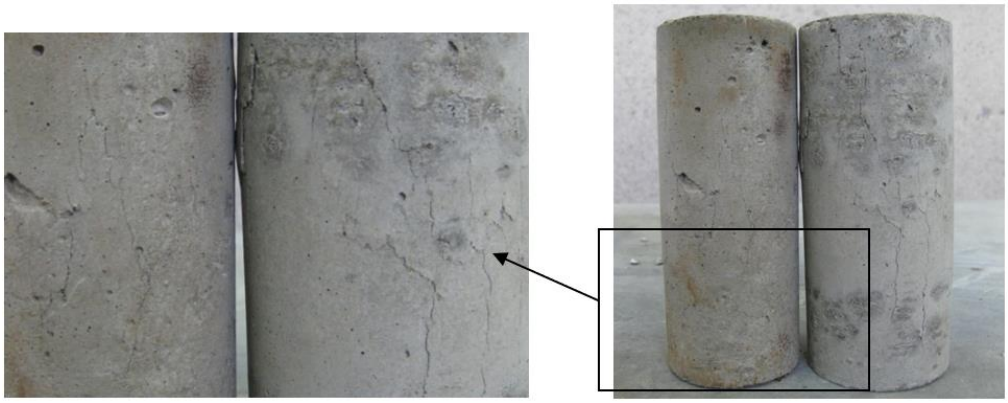

Fig. 8. Failure mode of unconfined concrete cores extracted from confined specimens on the test day.

3.1.2.Confined concrete specimens (Group F)

This section discusses the failure modes of various types of confinement, including FRP, steel, and hybrid FRP–steel systems. FRP-confined specimens (Group F) exhibited failure through rupture of the hoop fibers in the circumferential direction. This was triggered by significant lateral dilation of the core concrete, which generated high tensile stresses in the FRP jacket (Fig. 9(a)). The failure was typically sudden and brittle, characteristic of the limited ductility of FRP materials. Steel-confined specimens (Group S) failed due to radial bulging at mid-height without signs of local buckling. The steel tubes yielded under high circumferential tensile stress, with the most pronounced swelling occurring at the center of the specimen. This was attributed to the peak axial stress developing at mid-height and the friction between the specimen ends and the loading platens, which restrained lateral expansion near the ends (Fig. 9(b)). Hybrid FRP–steel confined specimens (Group SF) showed a sequential failure process. Initially, the FRP jacket ruptured in the hoop direction as a result of internal concrete expansion, reducing the confinement capacity. With continued axial loading, local buckling and eventual rupture of the steel tube followed, leading to a complete structural failure (Fig. 9(c)). This two-stage failure highlights the interaction and transitional behavior between brittle FRP and ductile steel confinement.

Table 1 summarizes the average compressive strength and ultimate axial strain for each group. Group F showed a ~2.3× strength increase and 10× higher strain than R'. Group S showed the highest strength, but Group SF achieved a better balance between strength and ductility. f_c' is unconfined compressive strength and f_{cc}' is confined compressive strength.

3.2. Stress-strain behavior

3.2.1.Axial stress–strain

The axial stress–strain curves of the specimens confined with steel tube (S), FRP (F), and hybrid FRP-steel tube (SF) demonstrated distinct behavioral differences, as shown in Fig. 10. Up to approximately the unconfined compressive strength ($f_c' \approx 24.7\ MPa$), all specimens exhibited a nearly identical response, indicating that lateral confinement does not activate significantly in the initial linear region of loading. Beyond this point, concrete begins to crack internally, generating lateral expansion that activates the confinement mechanism in each group. The stress–strain response then diverges based on the confinement system. The FRP-confined group (F) exhibited the steepest post-peak drop in stiffness, indicating more brittle failure, while the steel-confined

group (S) showed the most ductile behavior with a long post-peak plateau. The hybrid group (SF) showed intermediate behavior, benefiting from the stiffness of FRP and the ductility of steel.

(a) (b) (c)

Fig. 9. (a) Failure mode of an FRP-confined concrete specimen, (b) Failure mode of a steel tube-confined concrete specimen, and (c) Failure mode of a hybrid FRP–steel tube confined concrete specimen.

Table 1. Average Compressive Strength and Ultimate Axial Strain.

Group	f'_{cc} (MPa)	f'_{cc} / f'_c	Ultimate Axial Strain
R'	27.4	–	–
R	35.2	1.28	–
F	79.5	2.26	0.033
S	95.2	2.79	0.048
SF	89.7	2.61	0.026

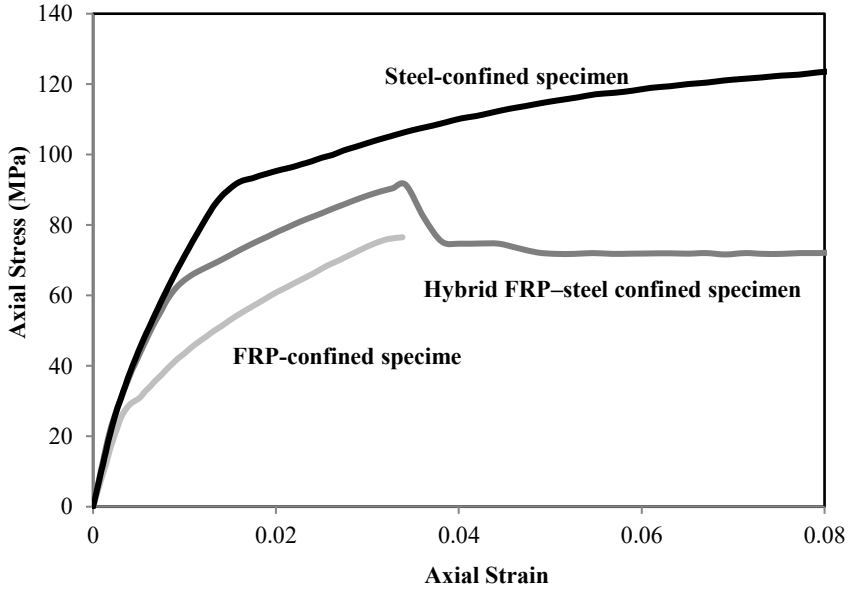

Fig. 10. Axial stress-strain curves of confined concrete specimens.

To further analyze this behavior, the lateral confining pressure f_l from elastic confinement can be calculated using the hoop stress relation:

$$f_\theta = E\varepsilon_\theta \quad \rightarrow \quad f_l = \frac{2tE\varepsilon_\theta}{D} = \left(\frac{2tE}{D}\right).\varepsilon_\theta \tag{5}$$

where E is the modulus of the confining material, ε_θ is the lateral strain, t is the thickness of the confining element, and D is the diameter of the concrete core. From Eq. 10, the equivalent lateral stiffness $\left(\frac{2tE}{D}\right)$ was calculated for each group to evaluate their contribution to lateral pressure resistance. For the FRP-confined group (F), the lateral stiffness was estimated at 0.8 GPa; for the steel-confined group (S), it was 7.2 GPa; and for the hybrid FRP–steel group (SF), the combined stiffness reached 15.1 GPa. These values confirm that the hybrid system offers the highest confinement effectiveness due to the parallel contribution of both FRP and

steel, while the FRP-alone system provides the lowest confinement stiffness, which explains its relatively more brittle behavior after peak stress.

To evaluate the initial stiffness of the confined specimens, the initial tangent modulus was calculated from the linear portion of the stress–strain curves. As illustrated in Fig. 11, the FRP-confined group (F) exhibited the lowest average elastic modulus, measured at 9699 MPa. In contrast, the steel-confined group (S) and hybrid group (SF) demonstrated higher initial stiffness values of 11,797 MPa and 11,655 MPa, respectively. This trend reflects the mechanical nature of the confining materials: while FRP primarily provides hoop confinement and does not significantly resist axial deformation, steel and hybrid tubes offer both axial and lateral stiffness. The slight difference between the S and SF groups suggests that the axial stiffness of the hybrid system is predominantly governed by the steel component. These findings confirm that FRP alone contributes less to axial stiffness, particularly during the early elastic stage, whereas steel and hybrid tubes enhance both the initial stiffness and the overall load-carrying behavior from the onset of loading.

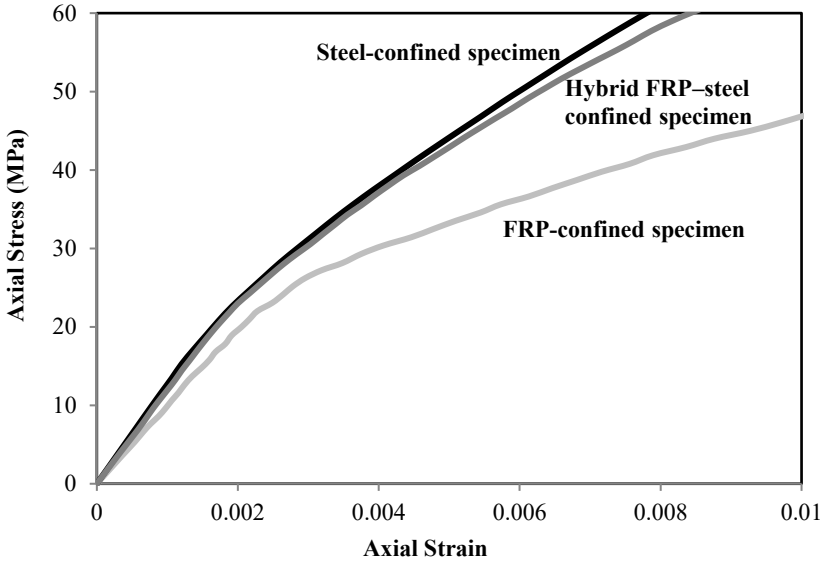

Fig. 11. Initial portion of axial stress-strain curves for confined concrete specimens.

3.2.2.FRP confinement

The stress–strain response of FRP-confined concrete specimens (Fig. 12) shows a distinct bilinear trend. In the initial phase, the behavior closely follows that of unconfined concrete, with the FRP jacket exerting minimal confinement. As the axial load increases, lateral expansion activates the FRP, which then begins to provide lateral pressure in a linear manner up to the rupture point. The slope of the second branch is primarily influenced by the hoop stiffness of the FRP and is only slightly affected by the compressive strength of the concrete. Increasing the number of FRP layers results in a higher confinement stiffness, thereby increasing the slope of the post-peak branch and raising the peak strength. Upon rupture of the FRP, the lateral confinement abruptly ceases, and since no further restraint is applied to resist lateral dilation, the core concrete fails suddenly. The failure is brittle and occurs at the moment of jacket rupture, highlighting the absence of post-rupture confinement.

3.2.3.Steel confinement

As shown in Fig. 13, steel-confined specimens behave differently. After the axial stress reaches the unconfined concrete strength, lateral expansion initiates hoop tension in the steel tube. Because of the high confinement stiffness of steel, there is only a minor drop in the curve's slope after the peak, and no significant post-peak softening is observed. The steel continues to apply nearly constant lateral pressure even after yielding, provided the steel demonstrates ideal elastic–plastic behavior. If the steel exhibits strain hardening, the lateral pressure increases post-yield, slightly raising the axial load capacity further. However, if the steel has low post-yield stiffness, the confinement effect declines more rapidly. In this study, the steel used showed noticeable strain hardening, contributing to improved ductility and a more stable post-peak response. The axial stress–strain curve remains smooth and transitions gradually into a softening branch.

3.2.4.Hybrid FRP–steel confinement

The hybrid specimens (Fig. 14) display a combined response. Initially, the confinement stiffness is high due to the contribution of both steel and FRP. At approximately 65 MPa axial stress, a sudden drop in slope occurs, which corresponds to the yielding of the steel tube. Although the steel's confinement contribution reduces after yielding, the FRP—still intact—continues to provide confinement and maintains the residual strength of the system. Once the FRP eventually ruptures, the lateral pressure from the hybrid shell decreases sharply. However, due to the ductility and strain capacity of the steel, the column maintains its integrity and prevents catastrophic failure. The steel tube absorbs deformation and preserves structural resistance over a wide strain range. This synergy between the brittle high-strength FRP and ductile steel results in a stable and staged failure mechanism, extending both the

strength and ductility of the system.

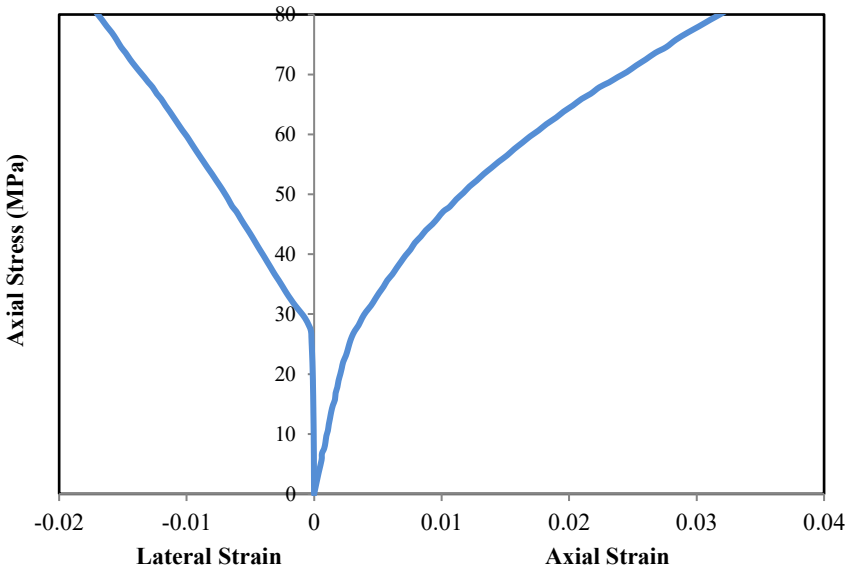

Fig. 12. Initial portion of axial stress-strain curves for confined concrete specimens.

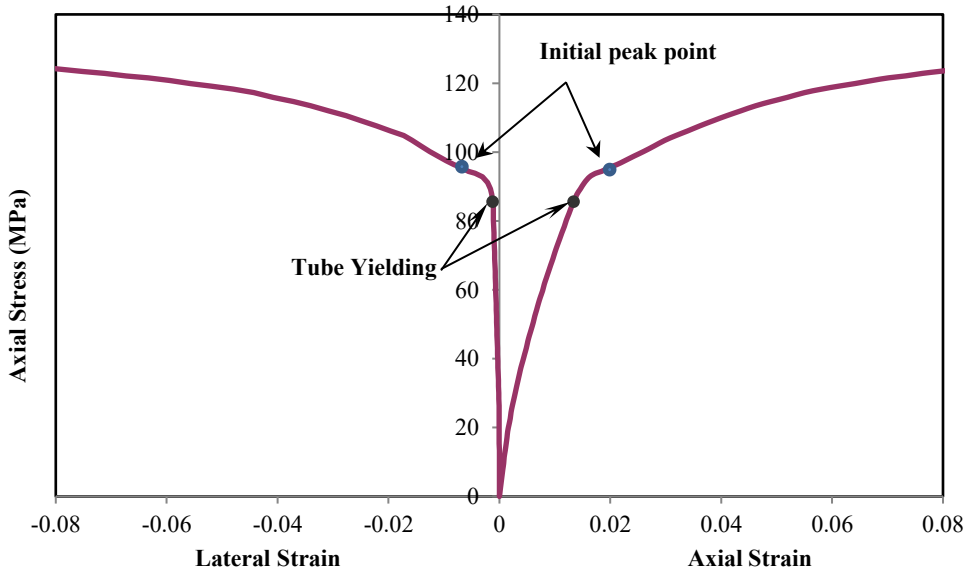

Fig. 13. Axial and lateral stress-strain curve of steel-confined concrete specimen, showing yielding and post-yield behavior.

3.3. Volumetric strain

Volumetric strain response was evaluated to gain a deeper understanding of the confinement effect in each group. The volumetric strain–axial stress curves are presented in Figs. 15 to 17 for the FRP, steel, and hybrid-confined specimens, respectively.

3.3.1.FRP-confined specimens

As shown in Fig. 15, the volumetric strain response of FRP-confined concrete begins with a positive slope, indicating a contraction behavior up to approximately the unconfined compressive strength f_c'. This phase corresponds to the compaction of internal voids and early crack closure. After reaching f_c', the slope turns negative, signifying a transition from contraction to dilation, as a result of increasing micro-cracking and internal damage. As the lateral strain increases, the internal pressure intensifies until it reaches the rupture limit of the FRP shell, causing a sudden drop in confinement. This rupture leads to a sharp and immediate increase in volumetric strain. Shortly after rupture, the curve exhibits a temporary rebound (i.e., a partial recovery of slope), reflecting the release of stored elastic energy in the FRP and concrete core. However, this recovery is short-lived, and the system soon transitions into a softening phase dominated by the rapid volumetric expansion of the now-unconfined concrete core.

3.3.2.Steel-confined specimens

The volumetric strain curve of the steel-confined specimen is illustrated in Fig. 16. Prior to the yielding of the steel tube, the behavior is predominantly contractive, and even after the axial stress reaches f_c', the core concrete remains well-confined. This is attributed to the high lateral stiffness of the steel tube, which effectively limits dilation. Once the steel yields, however, the rate of

lateral pressure increase slows down, and the volumetric strain curve shifts into the dilation region. Although strain hardening of the steel may delay this transition, it is not sufficient to entirely prevent it. As a result, post-yield volumetric expansion occurs, albeit less abruptly than in FRP-confined specimens.

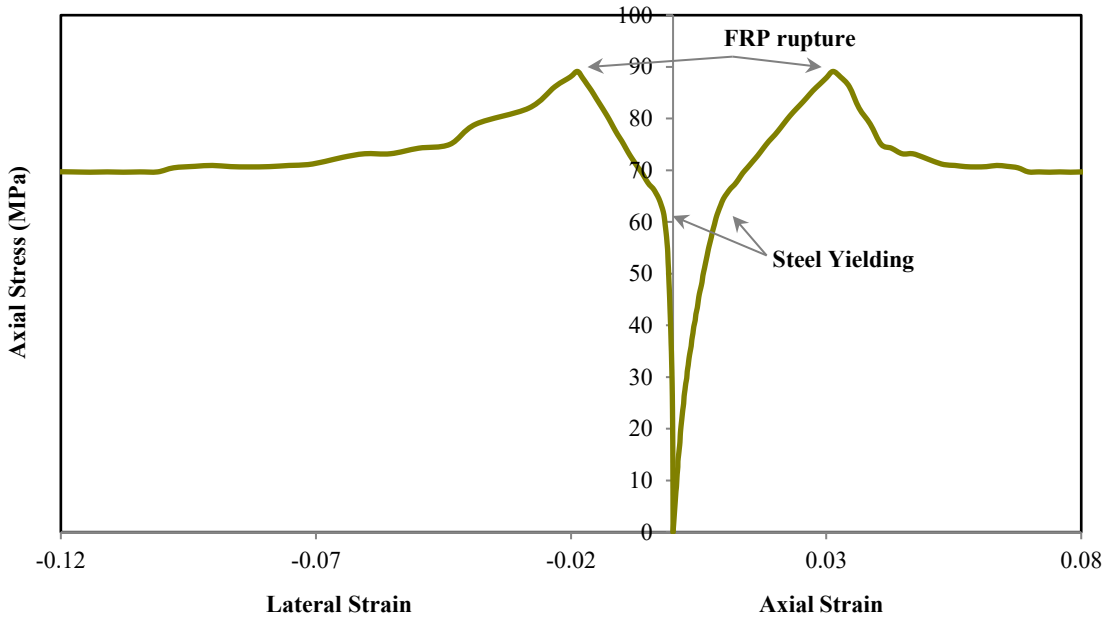

Fig. 14. Axial and lateral stress-strain response of a hybrid FRP–steel confined concrete specimen, indicating steel tube yielding followed by FRP rupture.

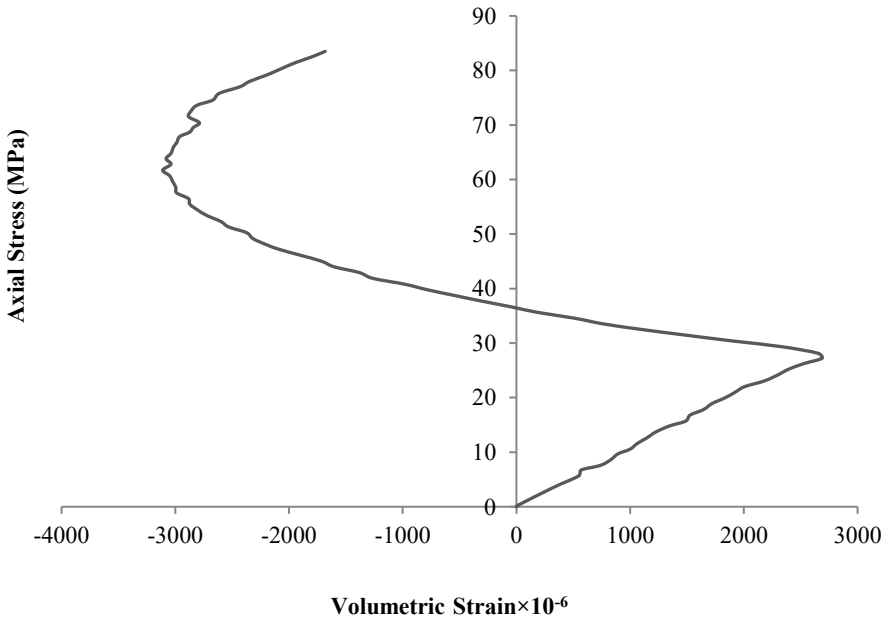

Fig. 15. Axial stress–volumetric strain curve of an FRP-confined concrete specimen.

3.3.3.Hybrid FRP–steel confined specimens

As shown in Fig. 17, prior to steel yielding, the hybrid-confined concrete exhibits a contractive volumetric behavior due to the high lateral stiffness of the combined FRP–steel tube. This confinement prevents noticeable internal cracking even at stress levels close to f_c'. Once the steel tube yields, the effective confinement stiffness drops significantly, resulting in a noticeable increase in volumetric strain and transition into the dilation phase. At this stage, microcracking and lateral deformation intensify. However, the rate of volumetric expansion is slower than in steel-only confined specimens because the FRP jacket remains intact and continues to apply lateral pressure. After the rupture of the FRP, the confinement capacity is significantly reduced, and the concrete core undergoes rapid lateral expansion. The post-rupture trend shows a steep increase in volumetric strain, confirming the loss of effective confinement and the onset of concrete softening under axial load.

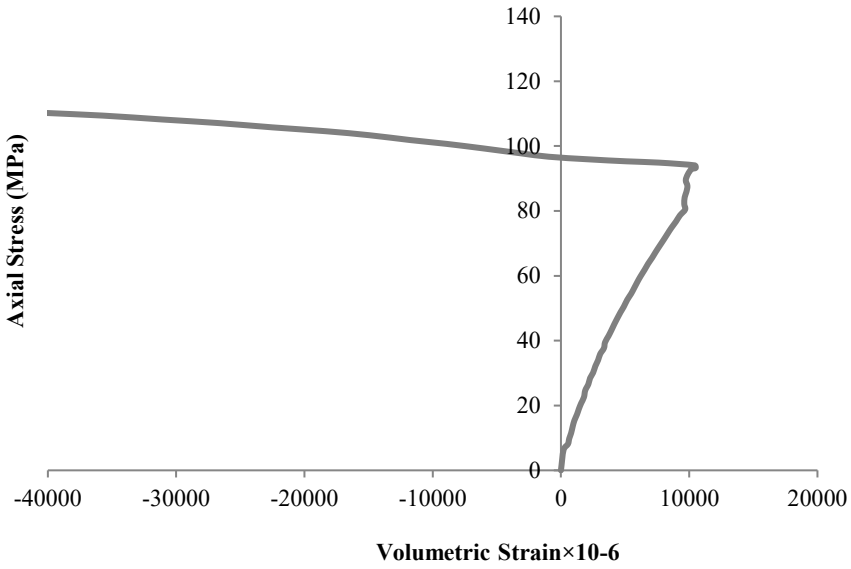

Fig. 16. Axial stress–volumetric strain curve of a steel-confined concrete specimen.

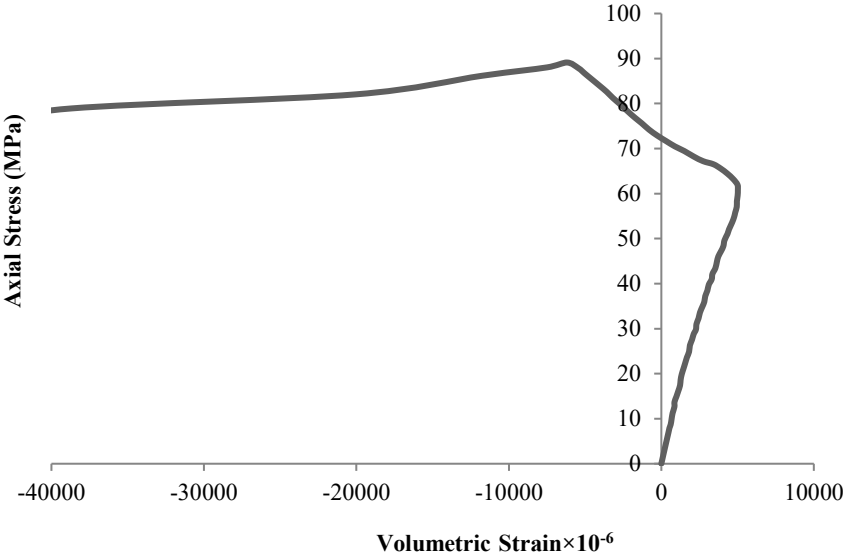

Fig. 17. Axial stress–volumetric strain curve of a hybrid FRP–steel confined concrete specimen.

4. Conclusion

This experimental study examined the axial behavior of concrete cylinders confined using steel tubes, FRP jackets, and hybrid FRP–steel tubes under identical confinement ratios. The comparison revealed distinct differences in failure mechanisms, stress–strain responses, and volumetric strain behavior across the confinement types.

In terms of failure mode, FRP-confined specimens failed suddenly due to brittle rupture of hoop fibers, while steel-confined specimens showed ductile bulging at mid-height. The hybrid specimens exhibited a staged failure sequence—initial FRP rupture followed by steel yielding and buckling—providing a more controlled and gradual failure process. The stress–strain behavior of the FRP group was bilinear with a sharp post-peak drop, indicating limited ductility. Steel-confined specimens maintained a smooth curve with extended post-peak strength due to strain hardening. Hybrid specimens demonstrated intermediate behavior, with high strength and improved post-peak ductility, reflecting the synergistic effect of FRP stiffness and steel ductility. Volumetric strain analysis confirmed these findings: FRP-confined specimens experienced rapid dilation post-rupture, while steel and hybrid groups exhibited more stable and restrained expansion. The hybrid group, in particular, delayed dilation onset and maintained better confinement after steel yielding and FRP rupture.

Overall, the hybrid FRP–steel system offered the most favorable balance between strength, ductility, and confinement effectiveness. It is recommended for applications demanding enhanced axial performance and failure control, particularly in seismic or durability-critical environments.

Statements & declarations

Author Contributions

Abolghasem Salari: Conceptualization, Investigation, Methodology, Formal analysis, Resources, Writing - Original Draft, Writing - Review & Editing.

Morteza Naghipour: Conceptualization, Methodology, Project administration, Supervision, Writing - Review & Editing.

Funding

The authors received no financial support for the research, authorship, and/or publication of this article.

Declarations

The authors declare no conflict of interest.

Data availability

The data presented in this study will be available on interested request from the corresponding author.

References

[1] Richart, F. E., Brandtzæg, A., Brown, R. L. A study of the failure of concrete under combined compressive stresses. Urbana (IL): University of Illinois, Engineering Experiment Station; 1928. Bulletin No.: 185.

[2] Newman, K., Newman, J. B. Failure theories and design criteria for plain concrete. In: Structure, Solid Mechanics and Engineering Design: Proceedings of the Southampton Civil Engineering Materials Conference; 1969; Southampton, UK. p. 963–995.

[3] Mander, J. B., Priestley, M. J. N., Park, R. Theoretical Stress-Strain Model for Confined Concrete. Journal of Structural Engineering, 1988; 114 (8): 1804–1826. doi:10.1061/(asce)0733-9445(1988)114:8(1804).

[4] Han, L. H., Liu, W., Yang, Y. F. Behavior of Thin Walled Steel Tube Confined Concrete Stub Columns Subjected to Axial Local Compression. Thin-Walled Structures, 2008; 46 (2): 155–164. doi:10.1016/j.tws.2007.08.029.

[5] Liu, J., Zhang, S., Zhang, X., Guo, L. Behavior and Strength of Circular Tube Confined Reinforced-Concrete (CTRC) Columns. Journal of Constructional Steel Research, 2009; 65 (7): 1447–1458. doi:10.1016/j.jcsr.2009.03.014.

[6] Qi, H., Guo, L., Liu, J., Gan, D., Zhang, S. Axial Load Behavior and Strength of Tubed Steel Reinforced-Concrete (SRC) Stub Columns. Thin-Walled Structures, 2011; 49 (9): 1141–1150. doi:10.1016/j.tws.2011.04.006.

[7] Lin, S., Zhao, Y. G., He, L. Stress Paths of Confined Concrete in Axially Loaded Circular Concrete-Filled Steel Tube Stub Columns. Engineering Structures, 2018; 173: 1019–1028. doi:10.1016/j.engstruct.2018.06.112.

[8] Xiamuxi, A., Zheng, T., Shao, J., Tan, T. Impact of Steel Tube Wall Thickness on Axial Compression Behavior of Reinforced and Recycled Aggregate Concrete-Filled Square Steel Tube Short Columns. Structures, 2024; 69: 107382. doi:10.1016/j.istruc.2024.107382.

[9] Cao, J., Jin, M., Chen, S., Ding, Q., Liu, J., Xiong, C., Jin, Z. Effect of Confinement of Steel Tube on Durability of Concrete Pier Exposed to Partial/Full Immersion Sulfate Attack Solution. Journal of Building Engineering, 2025; 99: 111477. doi:10.1016/j.jobe.2024.111477.

[10] Kurt, C. E. Concrete filled structural plastic columns. Journal of the Structural Division, ASCE. 1978; 104(1):55–63. doi:10.1061/jsdeag.0004849.

[11] Harmon T, Slattery K, Ramakrishnan S. The effect of confinement stiffness on confined concrete. In: Taerwe L, editor. Proceedings of the Second International RILEM Symposium (FRPRCS-2); 1995 Aug 23–25; Ghent, Belgium. Vol. 1. p. 584–592.

[12] Lam, L., Teng, J. G., Cheung, C. H., Xiao, Y. FRP-confined concrete under axial cyclic compression. Cement and Concrete Composites, 2006; 28(10): 949–958. doi:10.1016/j.cemconcomp.2006.07.007.

[13] Berthet, J. F., Ferrier, E., Hamelin, P. Compressive Behavior of Concrete Externally Confined by Composite Jackets: Part B: Modeling. Construction and Building Materials, 2006; 20 (5): 338–347. doi:10.1016/j.conbuildmat.2005.01.029.

[14] Li, G., Maricherla, D., Singh, K., Pang, S. S., John, M. Effect of Fiber Orientation on the Structural Behavior of FRP Wrapped Concrete Cylinders. Composite Structures, 2006; 74 (4): 475–483. doi:10.1016/j.compstruct.2005.05.001.

[15] Toutanji, H., Han, M., Matthys, S. Axial load behavior of rectangular concrete columns confined with FRP composites. In: Proceedings of the 8th International Symposium on Fiber-Reinforced Polymer Reinforcement for Concrete Structures (FRPRCS-8); 2007 Jul 16–18; Patras, Greece.

[16] Elsanadedy, H. M., Al-Salloum, Y. A., Alsayed, S. H., Iqbal, R. A. Experimental and Numerical Investigation of Size Effects in FRP-Wrapped Concrete Columns. Construction and Building Materials, 2012; 29: 56–72. doi:10.1016/j.conbuildmat.2011.10.025.

[17] Yang, Z., He, C., Kong, Q., Yuan, C. Monitoring the Microcrack Evolution in FRP-Wrapped Concrete Using Diffuse Ultrasound. Journal of Building Engineering, 2025; 109. doi:10.1016/j.jobe.2025.113009.

[18] Zheng, Y., Xu, F. H., Wang, D., Liang, M. Evaluating Ultimate Axial Strain Models for Concrete Square and Rectangular Columns Confined with FRP Composites. Journal of Physics: Conference Series, 2025; 3005 (1): 12008. doi:10.1088/1742-6596/3005/1/012008.

[19] Xiao, Y., He, W., Choi, K. Confined Concrete-Filled Tubular Columns. Journal of Structural Engineering, 2005; 131 (3): 488–497. doi:10.1061/(asce)0733-9445(2005)131:3(488).

[20] Feng, P., Cheng, S., Bai, Y., Ye, L. Mechanical Behavior of Concrete-Filled Square Steel Tube with FRP-Confined Concrete Core Subjected to Axial Compression. Composite Structures, 2015; 123: 312–324. doi:10.1016/j.compstruct.2014.12.053.

[21] Ma, L., Zhou, C., Lee, D., Zhang, J. Prediction of Axial Compressive Capacity of CFRP-Confined Concrete-Filled Steel Tubular Short Columns Based on XGBoost Algorithm. Engineering Structures, 2022; 260: 114239. doi:10.1016/j.engstruct.2022.114239.

[22] Liu, K. H., Xie, T. Y., Cai, Z. K., Chen, G. M., Zhao, X. Y. Data-Driven Prediction and Optimization of Axial Compressive Strength for FRP-Reinforced CFST Columns Using Synthetic Data Augmentation. Engineering Structures, 2024; 300: 117225. doi:10.1016/j.engstruct.2023.117225.